ChemPubSoc Europe

DOI: 10.1002/cssc.201500609

CHEMSUSCHEM Full Papers

Highly Active and Durable Nanocrystal-Decorated Bifunctional Electrocatalyst for Rechargeable Zinc–Air Batteries

Dong Un Lee, Moon Gyu Park, Hey Woong Park, Min Ho Seo, Xiaolei Wang, and Zhongwei Chen*[a]

A highly active and durable bifunctional electrocatalyst that consists of cobalt oxide nanocrystals (Co_3O_4 NC) decorated on the surface of N-doped carbon nanotubes (N-CNT) is introduced as effective electrode material for electrically rechargeable zinc–air batteries. This active hybrid catalyst is synthesized by a facile surfactant-assisted method to produce Co_3O_4 NC that are then decorated on the surface of N-CNT through hydrophobic attraction. Confirmed by half-cell testing, Co_3O_4 NC/N-CNT demonstrates superior oxygen reduction and oxygen evolution catalytic activities and has a superior electrochemical stability compared to Pt/C and Ir/C. Furthermore, rechargeable zinc–air battery testing of Co_3O_4 NC/N-CNT reveals superior galvanodynamic charge and discharge voltages with a significantly extended cycle life of over 100 h, which suggests its potential as a replacement for precious-metal-based catalysts for electric vehicles and grid energy storage applications.

Introduction

With ever-increasing concerns over the depletion of fossil fuel, the development of next-generation energy conversion and storage systems has become the main focus to improve global sustainability. As natural sources of energy are non-renewable, systems that generate energy using these sources are likely to become obsolete and will eventually be replaced by advanced rechargeable energy systems based on renewable energy sources. Among a variety of rechargeable energy systems, the lithium ion battery (LIB) is one of the most widely used systems because its advantages such as high energy efficiency, high power density, and good cycle stability.[1] However, the limitations of the LIB for further development are its relatively low specific energy density, the high cost of active materials, and safety concerns particularly for electric vehicle (EV) and hybrid electric vehicle (HEV) applications.[1–3] However, advanced battery systems such as metal-air batteries (MABs), which utilize freely available oxygen in the atmosphere, have gained much attention recently because of their extremely high energy density, environmental benignity, low cost, and safe operation.[1,3] As they utilize oxygen from the atmosphere, MABs do not require fuel reservoirs that allows a lightweight and compact battery design and fabrication, which are highly desirable for extending the driving range of EVs and HEVs. Among MABs, lithium–air batteries (LABs) and zinc–air batteries (ZABs) have been investigated rigorously and have very high theoretical energy densities (11 680 and 1084 Wh kg^{-1}, respectively).[1,3,4] However, ZABs in particular have attracted tremendous attention because of their safe operation, easy handling, and the abundance of zinc sources. ZABs also are very attractive for EV applications, in which safe operation is important, because of the nonexplosive and nonflammable properties of their components.[2] Despite these advantages, a few technical challenges must be addressed before the widespread commercialization of ZABs because of their limited practical energy density and insufficient cycle life as well as some technical challenges. Among many components of MABs, the development of the air electrode is one of the most critical areas especially to make it efficiently rechargeable mainly because of the sluggish kinetics of oxygen electrochemical reactions involved during the battery operation.[1,4–9] To make MABs properly rechargeable, the oxygen reduction reaction (ORR) and oxygen evolution reaction (OER), which are fundamental electrode reactions that govern the overall battery operation, must be catalyzed by a bifunctional oxygen electrocatalyst. Therefore, the development of highly active, durable, and cost-effective bifunctional electrocatalysts for air electrodes is critical for the future implementation of this technology. To date, noble-metal-based catalysts such as Pt and Ir on carbonaceous support materials (Pt/C and Ir/C) are currently the best ORR and OER electrocatalysts, respectively,[10–15] however, their severe scarcity, high prices, and insufficient electrochemical stability make them unsuitable for a wide range of practical applications.

To replace precious-metal-based catalysts, highly active and durable catalysts based on non-precious-metal or metal-free electrode materials have been developed.[1,2,6,13–24] For instance, Shanmugam et al. reported nanostructured 1 D $NiCo_2O_4$ spinel

[a] D. U. Lee,[+] M. G. Park,[+] Dr. H. W. Park, Dr. M. H. Seo, Dr. X. Wang, Prof. Z. Chen
Department of Chemical Engineering
Applied Nanomaterials&Clean Energy Laboratory
University of Waterloo
Waterloo, ON, N2L 3G1 (Canada)
E-mail: zhwchen@uwaterloo.ca

[+] These authors contributed equally to this work.

Supporting Information for this article is available on the WWW under http://dx.doi.org/10.1002/cssc.201500609.

© 2015 Wiley-VCH Verlag GmbH & Co. KGaA, Weinheim

oxides as an efficient bifunctional catalyst based on non-precious metals synthesized by utilizing the electrospinning technique for rechargeable zinc–air batteries.[25] Chen et al. introduced a metal-free carbon-based catalyst that consists of N-doped CNT and graphene as a highly active and durable bifunctional electrocatalyst.[7] In addition, by electrospinning then carbonizing a two-component polymer that consists of polystyrene (PS) and polyacrylonitrile (PAN), Cho et al. introduced highly porous N-doped carbon fibers as an efficient air electrode materials and explored the possibilities to utilize polymer alternatives for carbon nanotubes and graphene.[26] As an effective hybrid material for oxygen catalysis that combines non-precious transition metal oxides with active carbon nanostructures, Chen et al. synthesized perovskite oxides supported on two different structures, N-doped carbon nanotubes (N-CNT) and N-doped reduced graphene oxide (N-rGO), both which have shown high electrochemical activities toward the ORR and OER, comparable to state-of-art commercial Pt/C and Ir/C, respectively.[17,18] Schuhmann et al. suggested high-performance bifunctional composites composed of manganese oxide and cobalt oxide nanoparticles combined with N-doped carbon material. They employed high-temperature pyrolysis to obtain the bifunctional electrocatalysts using the unique structural and functional properties of precursor materials such as phthalocyanines.[15] However, hybrid catalysts are produced typically by synthesizing each component separately and then combining them by mechanical grinding or stirring, which leads to unfavorable interfaces and particle agglomeration to result in increased overpotentials during electrochemical reactions.

Herein, a simple synthetic strategy to produce hybrid catalysts effectively is introduced based on the hydrophobic attraction between cobalt oxide nanocrystals (Co_3O_4 NC) synthesized by surfactant-assisted interfacial self-assembly and the graphitic walls of N-CNT. This hybrid has been utilized in a practical rechargeable zinc–air single-cell battery prototype to show its efficient bifunctional catalytic properties (Scheme 1a).[27] The highly active Co_3O_4 NC/N-CNT hybrid catalyst has a uniform nanocrystal distribution that protects the CNT backbone. This new hybrid electrode material design is particularly interesting because of its simple preparation procedure that involves electrostatic interactions as the driving force without the use of high temperature or pressure. The hybrid catalyst is synthesized by a facile interfacial reaction in which Co_3O_4 NC are formed and become encapsulated by surfactant self-assemblies, which are then attached to the hydrophobic surfaces of N-CNT. Therefore, the final hybrid is composed of Co_3O_4 NC bound strongly by hydrophobic attraction and decorated uniformly on the surface of N-CNT, which results in an enhanced surface area with highly exposed catalytic active sites. To confirm the excellent electrochemical activities of the Co_3O_4 NC/N-CNT hybrid as an effective bifunctional electrode material, both half-cell and single-cell tests were performed by using the rotating disk electrode (RDE) technique and a rechargeable zinc–air battery prototype, respectively.

Results and Discussion

The TEM image and XRD pattern of Co_3O_4 NC, and SEM and TEM images of as-synthesized N-CNT are shown in Figure 1. The TEM image of Co_3O_4 NC shows cube-shaped nanocrystals with an average size of 5 nm and a good particle size uniformity (Figure 1a). The XRD pattern of Co_3O_4 NC is indicative of a cubic spinel crystal structure consistent with typical cobalt oxide nanoparticles (JCPDS no. 43–1003; Figure 1b).[6,16,28] The noise in the XRD pattern is caused by the very small dimensions of Co_3O_4 NC, however, the main peaks characteristic of spinel Co_3O_4 such as the (220), (331), and (511) reflections can be still observed. The SEM image of N-CNT reveals a uniformly grown tubular structure with a smooth outer surface that has an average diameter of ~50 nm and a length of several micrometers (Figure 1c). The TEM image of N-CNT supports the observations from the SEM image as bamboo-like structures are clearly visible that are attributed to defects at six-membered carbon rings in CNT (Figure 1d), which are generated by the five- and seven-membered ring construction because of the nitrogen dopants in the CNT.[29–32] SEM, TEM, and scanning transmission electron microscopy (STEM) images with color mapping from energy-dispersive X-ray (EDX) analysis of the Co_3O_4 NC/N-CNT hybrid are shown in Figure 2. In this work, our strategy to create a hybrid catalyst is based on the fast solvation-induced assembly of Co_3O_4/surfactant, which is attracted by a strong hydrophobic interaction onto the surface of N-CNT. The resulting hybrid shows Co_3O_4 NC still distributed uniformly onto the surfaces of N-CNT even after the removal of the surfactant (Figure 2a). A high-magnification TEM image of a single N-CNT shows that its surface is decorated uniformly with Co_3O_4 NC, and its bamboo-like morphology is also observed (Figure 2b). This hybrid material improves the morphology of Co_3O_4 particles grown hydrothermally from seed onto the surfaces of undoped multiwalled CNT reported previously in our group.[33] The formation of the unique morphology of the Co_3O_4 NC/N-CNT hybrid in this work is attributed to the two-phase-induced Co_3O_4 NC/surfactant system, which prevents aggregation and maintains the nanoscale particle size of the Co_3O_4 NC. A high-resolution TEM (HR-TEM) image was obtained to further examine the crystallinity of Co_3O_4 NC using a fast Fourier transform (FFT) pattern (Figure 2b inset),[6] which demonstrates the highly crystalline spinel structure of Co_3O_4 NC consistent with the XRD pattern. The adhesion of Co_3O_4 NC onto the surface of N-CNT is verified by STEM, and the elemental distribution is obtained by EDX as shown in the color maps (Figure 2c–e). The dashed rectangular area of the N-CNT surface decorated with Co_3O_4 NC resulted in purple-colored dots (Figure 2c). This shows the spread of cobalt oxide nanoparticles, which correspond to the small white particles (Figure 2d), and the yellow-colored dots show carbon species from N-CNT (Figure 2e). The yellow spots observed outside the rectangle are caused by the carbon-coated TEM copper grid.

Co_3O_4 NC decorated on Vulcan carbon (Co_3O_4 NC/VC), which is synthesized using the same method as Co_3O_4 NC/N-CNT, was investigated using TEM and SEM. Co_3O_4 NC/VC is employed as the control catalyst to elucidate the effect of the use of N-CNT

© 2015 Wiley-VCH Verlag GmbH & Co. KGaA, Weinheim

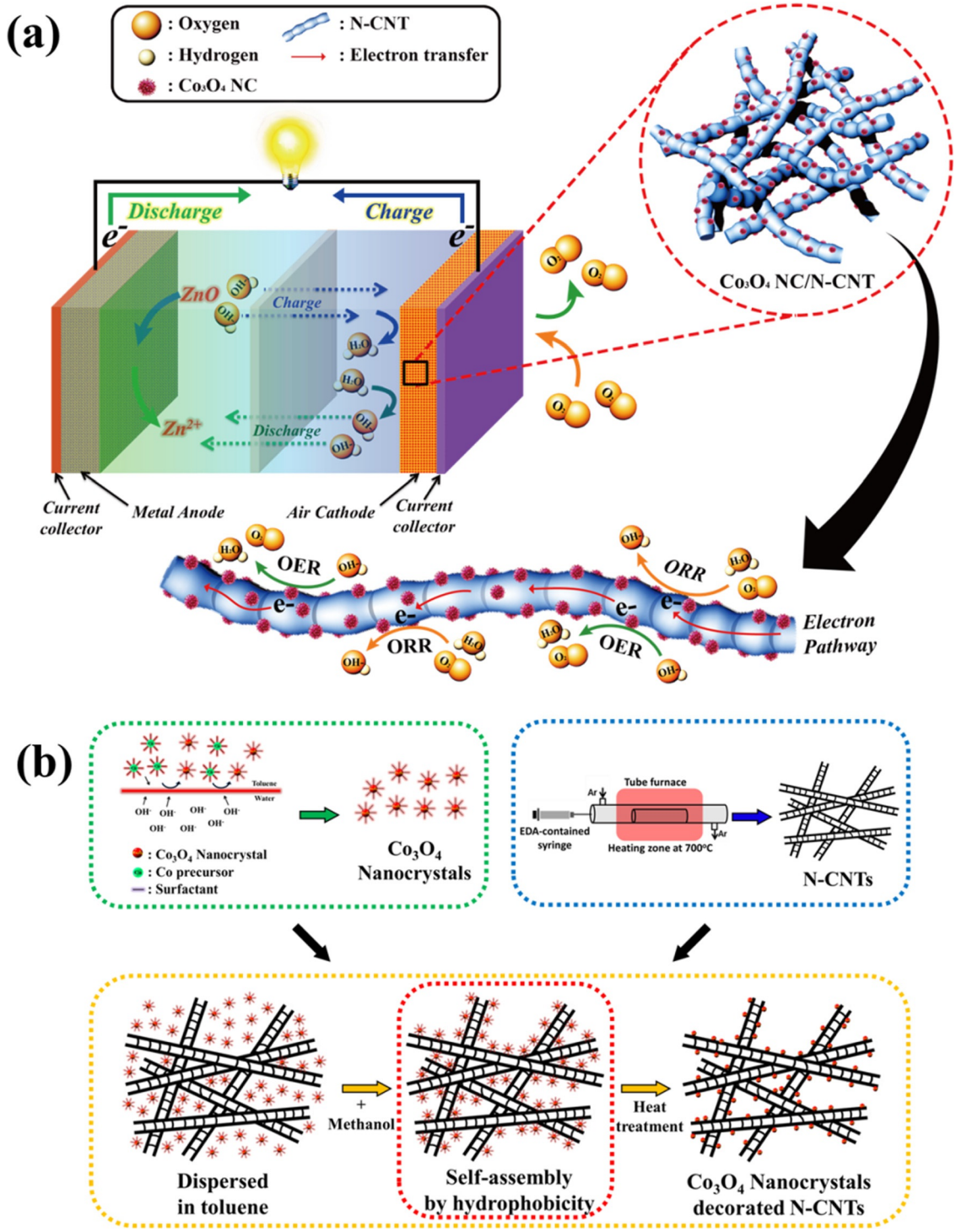

Scheme 1. (a) Schematic illustration of the charge and discharge processes of a zinc–air battery at the Co_3O_4 NC/N-CNT-coated GDL for bifunctional electrocatalysis for ORR and OER. (b) Diagram of the synthesis of Co_3O_4 NC/N-CNT by hydrophobic interactions.

as well as the synergistic effects between Co_3O_4 NC and N-CNT. It is also used to compare the morphological differences between the two respective carbon supports: N-CNT and VC (Figure S2). Similar to that of Co_3O_4 NC/N-CNT, Co_3O_4 NC are distributed well on the surface of VC particles. However, the VC particles themselves are observed to be aggregated, which reduces the overall exposure of active sites of Co_3O_4 NC. This is indicative of the effectiveness of N-CNT to enhance the exposure of the active sites of Co_3O_4 NC by creating an intertwined network because of its 1D morphology. The intertwined network of N-CNT has also been proven to be effective in terms of transporting charges during electrochemical oxygen reactions.[14]

© 2015 Wiley-VCH Verlag GmbH & Co. KGaA, Weinheim

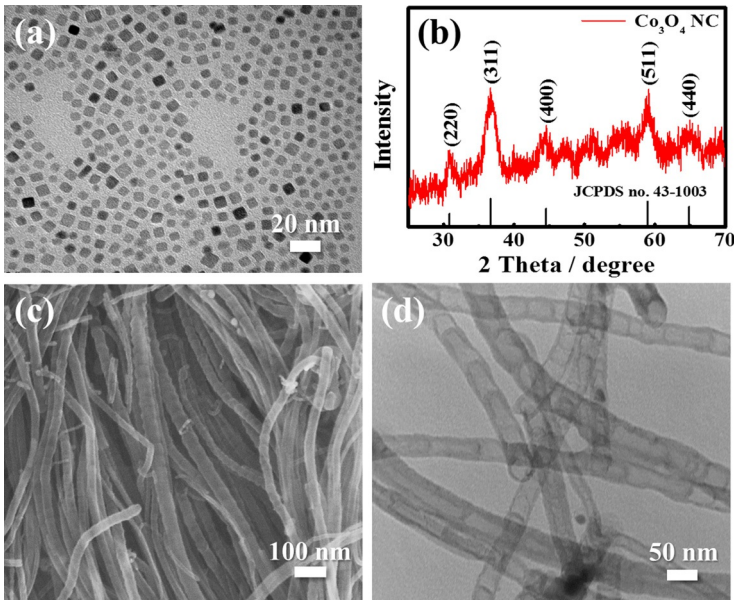

Figure 1. (a) TEM image and (b) XRD pattern of Co_3O_4 NC. (c) SEM and (d) TEM images of N-CNT.

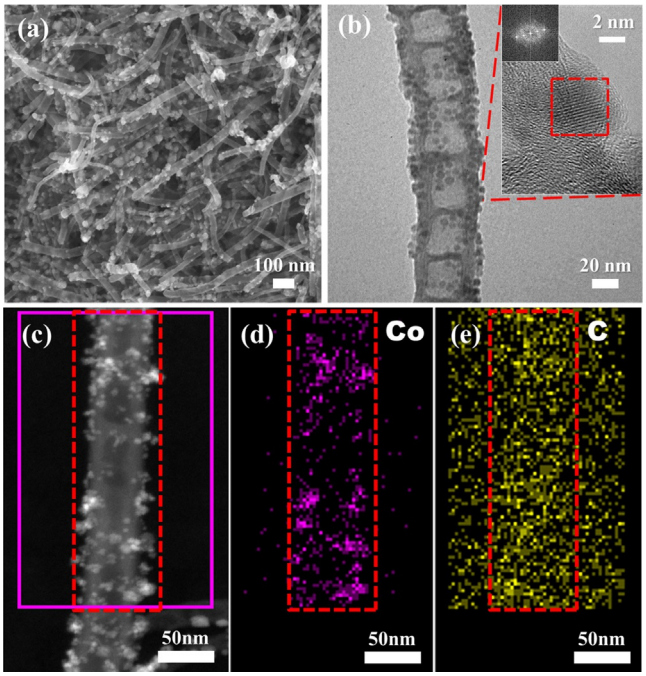

Figure 2. (a) SEM, (b) TEM, and (c) STEM images of Co_3O_4 NC/N-CNT. (d) Cobalt and (e) carbon color mapping images obtained from EDX of Co_3O_4 NC/N-CNT.

Thermogravimetric analysis (TGA) of Co_3O_4 NC/N-CNT was conducted in air to measure the amount of Co_3O_4 NC in the hybrid. A 45.7% weight reduction was observed over the temperature range of 300–450 °C because of the decomposition of N-CNT (Figure S3). As N-CNT has been etched to remove the leftover Fe from the injection chemical vapor deposition (CVD) growth before hybridization with Co_3O_4 NC, the amount of Co_3O_4 NC in the hybrid is determined to be 54.3%.

To further elucidate the elemental composition and catalytically active sites of the Co_3O_4 NC/N-CNT hybrid catalyst, X-ray photoelectron spectroscopy (XPS) was conducted. As expected, the full XPS survey of Co_3O_4 NC/N-CNT reveals peaks that correspond to Co 2p, Fe 2p, O 1s, N 1s, and C 1s (Figure 3a). The surface N content in N-CNT is confirmed to be 4.18%, which is consistent with CVD-grown N-CNT reported previously.[7,14,18] The high-resolution N 1s spectrum of Co_3O_4 NC/N-CNT was deconvoluted into a series of four peaks, which match the binding energies of different N-containing species such as pyridinic, pyrrolic, quaternary, and pyrrolidone closely (Figure 3b). The two species with the highest quantity, namely, pyridinic and pyrrolic, are 42.2 and 23.7% of the total, respectively. These ratio and binding energies of the surface N groups are consistent with N-CNT reported previously.[14,18] Among the four different N species, pyridinic and quaternary nitrogen species serve as the active site for the ORR.[11,34–36] This is appealing for combination with a highly active OER electrocatalyst such as Co_3O_4 to obtain a highly efficient bifunctional air electrode catalyst. The high-resolution Co 2p spectrum of the hybrid material has been deconvoluted into a series of six peaks, which are consistent with results reported previously (Figure S4).[37]

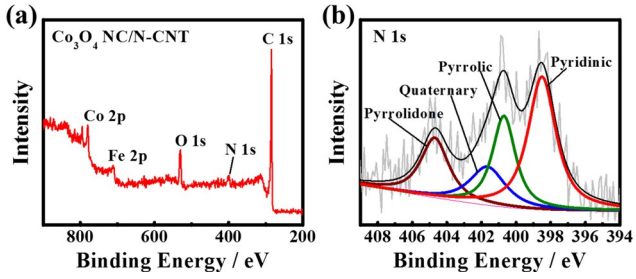

Figure 3. (a) The XPS survey and (b) high-resolution N 1s spectrum of Co_3O_4 NC/N-CNT composite: the grey and black lines are the raw and fitted spectra; the red, green, blue, and maroon lines are pyridinic-N (398.5 eV, 42.21%), pyrrolic-N (400.7 eV, 23.67%), quaternary-N (401.65 eV, 15.37%), and pyrrolidone-N (404.7 eV, 18.75%), respectively.

ORR polarization curves of Co_3O_4 NC/N-CNT, Co_3O_4 NC/VC, and N-CNT are shown in Figure 4a. Among the three, Co_3O_4 NC/N-CNT shows the most positive half-wave potential as well as the lowest overpotential, which are indicative of high electrochemical catalytic activity towards the ORR. Although Co_3O_4 NC/N-CNT has a lower N-CNT loading than N-CNT (because the total loading is kept the same), Co_3O_4 NC/N-CNT shows significantly improved onset and half-wave potentials. Even though the ORR of Co_3O_4 NC/N-CNT proceeds through the four-electron pathway, as determined by Koutecky–Levich (K-L) analysis (below), the slightly lower limiting current density obtained with Co_3O_4 NC/N-CNT than that of N-CNT is likely because of nonideal factors in the catalyst-coated layer on the glassy carbon such as film thickness resistance and trapped hydrogen

© 2015 Wiley-VCH Verlag GmbH & Co. KGaA, Weinheim

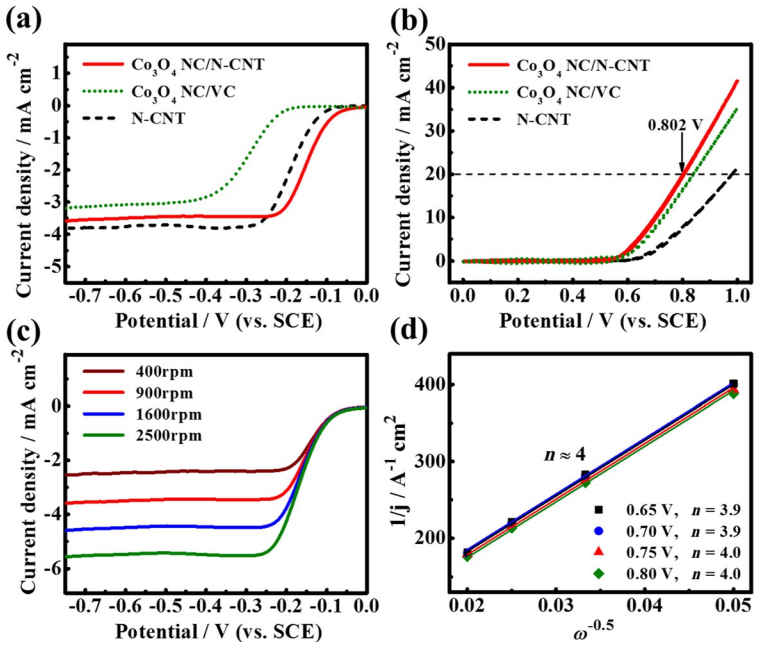

Figure 4. (a) ORR and (b) OER polarization curves of Co_3O_4 NC/N-CNT compared to Co_3O_4 NC/VC and N-CNT obtained at a rotation speed of 900 rpm. (c) ORR polarization curves of Co_3O_4 NC/N-CNT obtained at various rotating speeds (400, 900, 1600, and 2500 rpm). (d) K-L plot of Co_3O_4 NC/N-CNT hybrid obtained at 0.65, 0.70, 0.75, and 0.80 V. ORR and OER experiments were conducted in O_2- and N_2-saturated 0.1 M KOH, respectively.

peroxide species formed by the ORR catalyzed on Co_3O_4 NC within the electrode.[38,39] The combination of Co_3O_4 NC with N-CNT through hydrophobicity-induced coupling results in a superior ORR activity and signifies a strong synergistic effect between the two materials. Co_3O_4 NC/VC combined by the same method as Co_3O_4 NC/N-CNT lacks a significant ORR activity based on the considerably negative onset and half-wave potentials and reduced limiting current density. To investigate the bifunctionality of Co_3O_4 NC/N-CNT, the OER activity was investigated by cyclic voltammetry (CV) in the voltage range of 0–1 V vs. the saturated calomel electrode (SCE; Figure 4b). Of the three materials tested, the hybrid catalyst shows the best OER activity demonstrated by the highest OER current density of 42 mA cm^{-2} obtained at 1.0 V. Furthermore, Co_3O_4 NC/N-CNT shows the lowest overpotential of 0.802 V vs. SCE obtained at 20 mA cm^{-2}. Even though Co_3O_4 NC/VC demonstrates the same onset potential (~0.57 V vs. SCE), the OER current density at 1.0 V is only 35 mA cm^{-2}. The ORR and OER activities of the three catalysts are summarized in Table S1. The synergistic combination of Co_3O_4 NC and N-CNT by hydrophobicity-induced coupling is again demonstrated for the OER, in which N-CNT shows a poor onset potential and a low current density. With the addition of Co_3O_4 NC, the OER onset potential and current density were improved significantly. The two materials are synthesized from the same Co_3O_4 NC and are utilized as OER-active electrocatalysts. However, due to different natures of carbon supports utilized, VC leads to the decrease in exposed active sites for OER, whereas N-CNT enhances overall electrical conductivity by acting as a bridge for electron transfer and increases active site exposure for improved OER.

To further understand the excellent ORR kinetics of the Co_3O_4 NC/N-CNT hybrid catalyst, K-L analysis was conducted at various electrode potentials (0.65, 0.70, 0.75, and 0.80 V; Figure 4d) based on the Koutecky–Levich equation (Supporting Information) using ORR measurements obtained by using a RDE at four different rotation speeds of 400, 900, 1600, and 2500 rpm (Figure 4c). These parallel and linear fitting lines indicate first-order reaction kinetics towards the saturated oxygen species. The number of electrons transferred, *n*, during the ORR is 3.9, 3.9, 4.0, and 4.0 at potentials of 0.65, 0.70, 0.75, and 0.80 V vs. SCE, respectively. This indicates fast kinetics with a predominant four-electron reduction reaction mechanism throughout the entire potential range inspected. This high activity towards the ORR is attributed to the synergy between Co_3O_4 NC and N-CNT, and the coupling of the two by strong hydrophobic interactions improved the active surface area and charge transport properties. To emphasize the potential use of Co_3O_4 NC/N-CNT hybrid catalyst for practical applications, its ORR and OER activities are compared to those of commercial state-of-the-art catalysts, Pt/C and Ir/C (Figure S5a and b, respectively). As Pt/C and Ir/C are known to be monofunctionally active towards the ORR and OER, respectively, the two w mixed physically in a 1:1 ratio to create a bifunctionally active counterpart. The ORR measurements of the catalysts reveal that even though the mixture of Pt/C and Ir/C outperforms Co_3O_4 NC/N-CNT slightly in terms of onset and half-wave potentials and limiting current density, the cost effectiveness of the hybrid catalyst compensates for the sacrificed performance. Similarly, the OER activity of the mixture of Pt/C and Ir/C outperforms that of Co_3O_4 NC/N-CNT slightly in terms of onset potential and OER current density. The ORR and OER activities of the composite can be further enhanced by introducing a second transition metal such as $NiCo_2O_4$ and the co-doping of carbon nanotubes, such as S,N-doped carbon nanotubes, to outperform Pt/C and Ir/C, which will be investigated in our future work.

In addition to the ORR and OER activities of Co_3O_4 NC/N-CNT, the electrochemical durability of the hybrid catalyst has been investigated to further highlight its potential application in practical rechargeable metal–air batteries (Figure 5). The electrochemical durability is tested by conducting repeated CVs in the range of 0–1 V vs. SCE to expose the catalyst to severely oxidative conditions. Even after 1000 cycles, the Co_3O_4 NC/N-CNT hybrid catalyst shows a relatively low decrease in current density at 1 V vs. SCE (Figure 5a), whereas Co_3O_4 NC/VC, N-CNT, and the mixture of Pt/C and Ir/C demonstrate a significant reduction in current density (N-CNT only after 300 cycles; Figure 5b, c, and d and Table S1). Even though Co_3O_4 NC helps to reduce the overpotential associated with OER for both the N-CNT- and VC-supported hybrids, Co_3O_4 NC/N-CNT demonstrates a much higher current density retention (91.2%) than Co_3O_4 NC/VC (40.7%) because of the graphitized carbon in N-CNT, which is known to be electrochemically very

© 2015 Wiley-VCH Verlag GmbH & Co. KGaA, Weinheim

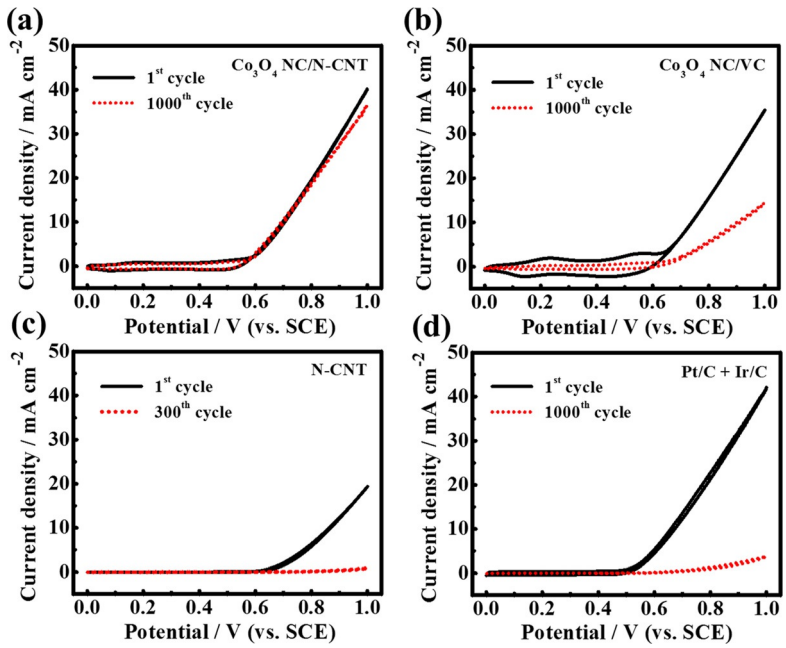

Figure 5. The first and 1000th CV cycle in the OER region obtained with (a) Co_3O_4 NC/N-CNT, (b) Co_3O_4 NC/VC, (c) N-CNT (300th) and (d) Pt/C+Ir/C.

stable.[40–42] In addition, the improved durability is ascribed to the morphological advantage of the highly intertwined network of 1D carbon nanotubes over the granular morphology created by VC.[18] Although the mixture of Pt/C and Ir/C shows a superior initial activity to Co_3O_4 NC/N-CNT, it demonstrates a poor durability, which highlights the hybrid catalyst as a potential replacement for practical applications. The decrease of current density for Pt/C and Ir/C is most likely attributed to the corrosion of carbon during exposure to high charging potentials, however, Co_3O_4 NC/N-CNT is significantly less affected because of the synergistically enhanced catalytic activity, which prevents N-CNT from prolific corrosion.[1,14,18]

To corroborate the excellent bifunctional activities of Co_3O_4 NC/N-CNT confirmed by half-cell testing, a rechargeable zinc–air cell prototype was fabricated, and the hybrid material was tested as the air electrode catalyst to emphasize its electrocatalytic performance in a realistic environment. The zinc–air battery performance of the catalysts was investigated by conducting galvanodynamic charge and discharge tests to observe the behavior of battery operation in terms of voltage for a wide range of applied (or drawn) current densities (Figure 6a). The open-circuit voltages of Co_3O_4/N-CNT and N-CNT are comparable and higher than that of Co_3O_4 NC/VC because of the superior electrical conductivity of the CNT. In terms of discharge, Co_3O_4 NC/N-CNT demonstrates the best discharge performance as evidenced by the highest discharge voltages obtained at all tested current densities. The differences in the discharge voltage become clearer at high current densities, which is indicative of the superior rate capability of Co_3O_4 NC/N-CNT. The trend in the observed discharge performance is consistent with that of the half-cell testing in which N-CNT shows a better performance than Co_3O_4 NC/VC, most likely because of the fast charge transport facilitated by the highly electrically conductive CNT. During battery charging, Co_3O_4 NC/N-CNT demonstrates best overall OER performance with significantly lower charging potentials particularly at high current densities.

In addition to the galvanodynamic charging and discharging behaviors of the catalysts, electrochemical impedance spectroscopy (EIS) was conducted in the ORR region at 0.8 V to further investigate the resistances associated with rechargeable zinc–air battery operation (Figure 6b, inset). EIS testing resulted in Nyquist plots composed of two different sized semicircles, which are modeled by an equivalent circuit with five parameters, R_s, R_{int}, R_{ct}, Q_{int}, and Q_{dl}, consistent with our zinc–air battery results reported previously.[14,18,37] Each resistance has its own physical interpretation. R_s represents solution resistance in the electrolyte, and R_{int} represents

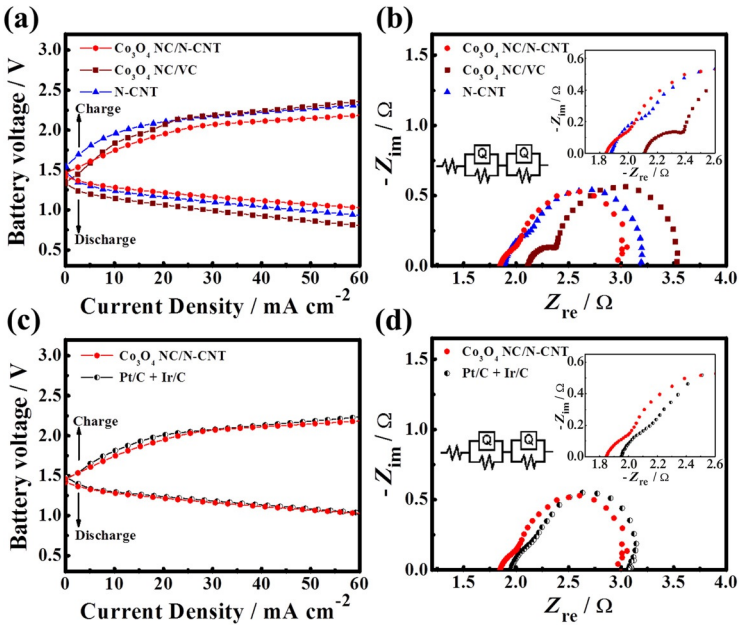

Figure 6. a, c) Galvanodynamic charge and discharge behaviors. b, d) Nyquist plots obtained by EIS of Co_3O_4 NC/N-CNT (red circle), Co_3O_4 NC/VC (maroon hexagon), N-CNT (blue triangle), and Pt/C+Ir/C (black half circle). Insets in (b) and (d): High-frequency range of the Nyquist plot and the equivalent circuit.

© 2015 Wiley-VCH Verlag GmbH & Co. KGaA, Weinheim

solid–electrolyte interface resistance between the solid and liquid of the electrode. R_{ct} represents charge-transfer resistance from the air electrode, which is related directly to the catalytic activity of the catalyst. Q_{int} and Q_{dl} correspond to interfacial and double layer constant phase elements (CPEs), respectively. Based on the equivalent circuit, the impedance parameters of each catalyst are listed in Table 1, and Co_3O_4 NC/N-CNT exhibits a lower charge-transfer resistance than Co_3O_4 NC/VC and N-CNT, which is consistent with the results obtained from the galvanodynamic discharge test. The hybrid also presents the lowest values of R_s and R_{int}, which is because of the addition of highly electrically conductive N-CNT and the excellent distribution of Co_3O_4 NC on the surfaces of N-CNT, respectively. Based on the outstanding charge–discharge performance and impedance results of Co_3O_4 NC/N-CNT, a physical mixture of Pt/C and Ir/C commercial catalysts was tested to compare the viability of the hybrid catalyst as a potential commercial electrode material (Figure 6c and d, inset). The galvanodynamic charge and discharge of Co_3O_4 NC/N-CNT is comparable to that of the Pt/C and Ir/C mixture, which is demonstrated by the similar charge and discharge voltages throughout the tested current densities. The excellent performance of the hybrid is confirmed by EIS, as all three resistances, R_s, R_{int}, and R_{ct}, are lower than those of the precious-metal-based catalyst (Table 1).

Table 1. Values of the equivalent circuit elements based on the EIS analysis of Co_3O_4 NC/N-CNT, Co_3O_4 NC/VC, N-CNT, and a mixture of Pt/C and Ir/C.

Catalyst	Initial cycle					After cycling				
	resistance [Ω]			CPE [S s^n]		resistance [Ω]			CPE [S s^n]	
	R_s	R_{int}	R_{ct}	Q_{int}	Q_{dl}	R_s	R_{int}	R_{ct}	Q_{int}	Q_{dl}
Co_3O_4 NC/N-CNT	1.849	0.199	1.026	0.0105	0.01349	2.443	0.721	1.902	2.41×10^{-3}	5.71×10^{-3}
Co_3O_4 NC/VC	2.116	0.284	1.139	0.002425	0.01178	3.28	0.726	10.97	0.2879	1.56×10^{-3}
N-CNT	1.887	0.264	1.061	0.00565	0.01366	2.677	0.511	3.967	6.44×10^{-3}	7.91×10^{-3}
Pt/C+Ir/C	1.954	0.236	1.046	0.01462	0.0274	3.189	0.402	4.686	2.57×10^{-3}	5.83×10^{-3}

To further support the excellent charge and discharge capabilities of Co_3O_4 NC/N-CNT as a bifunctional air electrode catalyst for rechargeable zinc–air batteries, its cycle stability was investigated by charging and discharging the battery galvanostatically at 20 mA cm^{-2} (Figure 7). As expected, the battery with Co_3O_4 NC/N-CNT shows very stable charge and discharge voltages, 2.16 and 1.14 V, respectively, which demonstrates virtually negligible voltage fading for more than 200 cycles (2000 min) (Figure 7a). The cycle stability of other batteries with Co_3O_4 NC/VC, N-CNT, and the mixture of Pt/C and Ir/C, however, demonstrated significant voltage losses only after ~40 cycles before the batteries were stopped because of very high overpotentials (Figure 7b, c, and d). The voltage losses in these batteries are mainly attributed to the corrosion of carbon, which is caused by high charge voltages. This leads to the loss of the catalytically active surface area and the poisoning of the electrolyte, which results in the loss of discharge voltages. The rate of charge voltage loss is more severe for Co_3O_4 NC/VC than N-CNT because of the amorphous nature of VC, whereas the graphitic carbon of N-CNT mitigates the rate of degradation. Similarly, the mixture of Pt/C and Ir/C demonstrates severe degradation in terms of both charge and discharge voltages even though its initial performance is superior. Furthermore, the initial four cycles of the charge–discharge profiles of Co_3O_4 NC/VC, N-CNT, and the mixture of Pt/C and Ir/C demonstrate high overpotentials, whereas Co_3O_4 NC/N-CNT shows a relatively narrow difference between the charge–discharge voltages (inset in Figure 7b, 7, and d, respectively). This galvanostatic cycling test is indicative of the importance to have both stable graphitic carbon and highly OER-active Co_3O_4 NC to minimize charge–discharge voltage degradation. To further confirm the durability of the hybrid catalyst, a long-term galvanostatic charge–discharge cycling test was conducted using a 4 h cycling interval (2 h discharge then 2 h charge) at the same current density (Figure 8). Even though this leads to harsh testing conditions for the catalyst in terms of electrochemical durability, the battery exhibits very stable voltages over 100 h (350000 s). This result obtained with long charging and discharging regimes demonstrates the potential use of the highly active and durable Co_3O_4 NC/N-CNT hybrid bifunctional catalyst as an efficient air electrode material for real applications. After the galvano-

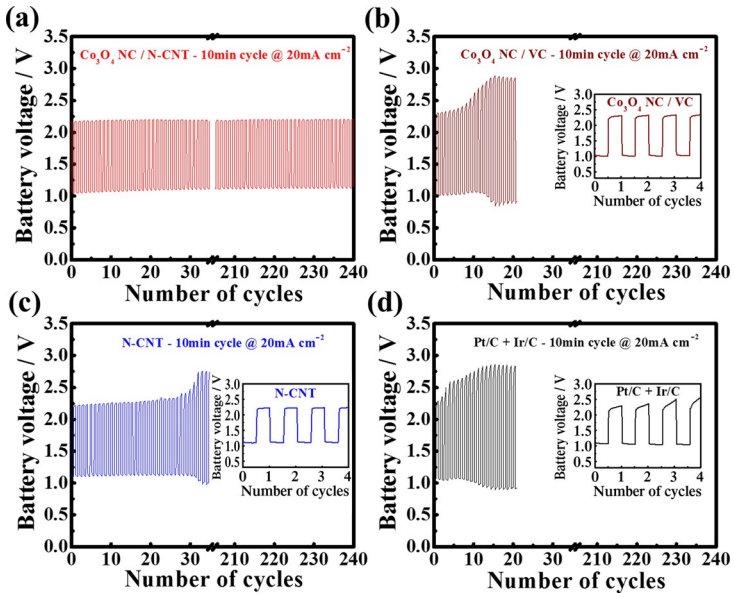

Figure 7. Galvanostatic charge–discharge cycling obtained at 20 mA cm^{-2} for (a) Co_3O_4 NC/N-CNT, (b) Co_3O_4 NC/VC, (c) N-CNT, and (d) Pt/C+Ir/C. Insets: The initial four cycles of each catalyst.

© 2015 Wiley-VCH Verlag GmbH & Co. KGaA, Weinheim

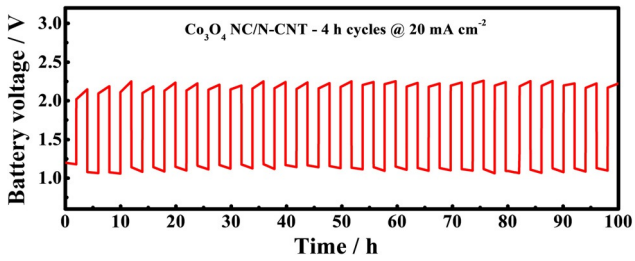

Figure 8. Long-term galvanostatic charge–discharge cycling obtained at 20 mA cm^{-2} for Co_3O_4 NC/N-CNT. Each charge and discharge state was 2 h (4 h per cycle).

static cycling tests, the same batteries were tested for galvanodynamic charge and discharge to further verify the durability of the catalysts (Figure S6 a and c). Co_3O_4 NC/VC suffers from the largest charge and discharge performance loss compared to its initial performance observed by the greater increase in charge and discharge overpotentials. The Co_3O_4 NC/N-CNT hybrid catalyst shows the smallest decrease and increase in the discharge and charge voltage, respectively, which elucidates the electrochemical stability with highly active bifunctional properties. The bifunctional mixture of Pt/C and Ir/C also displays a considerably enlarged charge/discharge voltage difference in contrast to that of the hybrid material. The order of the increased overpotential between the charge and discharge profiles from that at the initial stage is Co_3O_4 NC/N-CNT < N-CNT < Pt/C+Ir/C < Co_3O_4 NC/VC, which corresponds to 0.297, 0.501, 0.883, and 1.126 V, respectively, at a relatively high current density of 50 mA cm^{-2} (Tables S2 and S3). With respect to electrochemical resistances in the zinc–air battery single cell, EIS was conducted at the last stage after charge–discharge cycling experiments as displayed by the Nyquist plots (Figure S6 b and d). In agreement with the trend of the increasing overpotentials before and after the galvanostatic charge and discharge cycling test, the increase in the electrochemical resistances is observed in the order of Co_3O_4 NC/N-CNT < pure N-CNT < Pt/C+Ir/C < Co_3O_4 NC/VC. Conclusively, all of electrochemical characterizations such as half-cell testing, galvanodynamic and galvanostatic charge and discharge, and EIS demonstrate a consistent durability trend among the catalysts. In comparison with the other electrocatalysts, Co_3O_4 NC/N-CNT has a strong electrochemical durability and excellent rechargeability as well as a highly active and bifunctional performance in both half-cell testing and zinc–air battery cycling experiments.

Conclusions

A facile synthesis method to decorate cobalt oxide nanocrystals (Co_3O_4 NC) onto the surface of N-doped carbon nanotubes (N-CNT) is introduced based on hydrophobicity-induced solvation to obtain a highly active Co_3O_4 NC/N-CNT hybrid electrocatalyst. The catalyst is formed by the strong hydrophobic interactions between surfactants that encapsulate the Co_3O_4 NC and the graphitic walls of the N-CNT. From rotating disk electrode half-cell testing and practical rechargeable zinc–air battery measurements, the synergistic effect of the Co_3O_4 NC/N-CNT hybrid catalyst is verified by comparing it to Co_3O_4 NC/VC and N-CNT, which demonstrate relatively lower bifunctional activities. The oxygen reduction reaction (ORR) and oxygen evolution reaction (OER) activity of the hybrid catalyst compared to those of precious-metal-based catalysts such as Pt/C and Ir/C, respectively, highlights its potential for usage in practical applications. The synergistic effect is obtained from the hydrophobic combination between N-doped CNT, which mainly provides highly active ORR sites and the exceptional electrical conductivity for rapid charge transfer, and Co_3O_4 NC, which provides highly exposed OER active sites. In addition to the high bifunctional activity, Co_3O_4 NC/N-CNT exhibits remarkably stable OER polarization curves at a very high potential range between 0 and 1 V (vs. standard calomel electrode) and sustains more than 90% in OER current retention even after 1000 cyclic voltammetry cycles. The practicality of the hybrid catalyst is further elucidated by its excellent cycling durability as well as the low overpotential between charge and discharge performances in a realistic rechargeable zinc–air battery under ambient conditions. As a result of the simple and facile synthesis of the nanocrystals with N-CNT, the Co_3O_4 NC/N-CNT hybrid catalyst is highly promising for next-generation rechargeable batteries such as metal–air batteries and alkaline full cells.

Experimental Section

Chemicals and materials

All of chemicals were purchased from Sigma–Aldrich and used without further processing. Cobalt nitrate hexahydrate, sodium stearate, methanol, toluene, dodecylamine, and *tert*-butylamine were employed for the synthesis of Co_3O_4 NC, ethylenediamine and ferrocene were utilized for N-CNT, and sulfuric acid was used to etch the N-CNT.

Catalyst preparation

Synthesis of N-CNT: N-CNT were prepared by a simple injection CVD method as described previously.[7] Briefly, ethylenediamine (EDA) and ferrocene were employed as the carbon source and catalyst, respectively. First, EDA and ferrocene were dissolved in ethanol by ultrasonication for 2 h to obtain a homogeneous dispersion. Then, a tube furnace was set up with a large quartz tube, a syringe pump, and a syringe, which was filled with EDA solution (2 mL). The furnace was heated to 700 °C at which point the syringe pump was turned on to begin injecting the precursor solution for 40 min with a flow rate of 0.05 mL min^{-1}. Once the injection was finished, the pump was turned off and the furnace was cooled to RT after heating at 700 °C for total of 2 h. N-CNT was obtained by collecting black powder from the quartz tube. N-CNT was then acid-treated in 0.5 M H_2SO_4 solution to remove impurities including Fe particles. After acid etching, N-CNT were washed and filtered using doubly deionized (DDI) water and dried at 60 °C.

Synthesis of Co_3O_4 NC: Co_3O_4 NC were prepared by a simple two-phase hydrothermal synthesis.[28,43] Cobalt stearate ($Co(SA)_2$), which was used as a precursor, was first prepared for synthesis of Co_3O_4 NC. In a typical synthesis, an oil-phase mixture of toluene (15 mL), dodecylamine (1.0 g), and Co(SA)2 (0.15 g) in a vial was heated at 90 °C until the solution become optically clear. Then the solution

© 2015 Wiley-VCH Verlag GmbH & Co. KGaA, Weinheim

was cooled to RT and loaded into a 50 mL Teflon liner. Deionized water (15 mL) and *tert*-butylamine (150 μL) were mixed to prepare a water-phase solution, which was added to the 50 mL Teflon liner before the addition of the oil-phase solution. The two-phase solution was heated in the autoclave without stirring at 180 °C for 5 h. After the autoclave reaction was finished and cooled to RT, the solution that contained Co_3O_4 NC was poured from the Teflon liner into a test tube and mixed with methanol (30 mL) to induce the precipitation of Co_3O_4 NC. Finally, Co_3O_4 NC were separated by centrifugation and washing with methanol solution and stored in a toluene solution, which was utilized as a redispersion agent for Co_3O_4 NC because of its hydrophobic properties.

Preparation of Co_3O_4 NC/N-CNT: Simple self-assembly was employed to obtain the hybrid catalyst.[44] As-prepared N-CNT were first dispersed into the Co_3O_4 NC solution under ultrasonication for 2 h. Then methanol was added into the mixture, which created a strong hydrophobic interaction between the two components that thereby self-assembled into the Co_3O_4 NC/N-CNT hybrid. The precipitated composite was separated by vacuum filtration and dried completely at 50 °C. Finally, the dried composite was heat treated at 450 °C for 2 h under Ar to obtain strong coupling between Co_3O_4 NC and N-CNT and eliminate any remaining surfactants between the two components. Co_3O_4 NC/VC employed as a reference material was prepared using vulcan carbon (Vulcan XC-72) instead of the N-CNT from the same synthesis. The overall synthesis of Co_3O_4 NC, N-CNT, and Co_3O_4 NC/N-CNT is illustrated in Scheme 1 b.

Materials characterization

For chemical and physical characterization of the prepared materials, a variety of techniques were employed. SEM (LEO FESEM 1530) and TEM (JEOL 2010F) images were obtained to investigate the surface structure and morphology of the prepared materials. Furthermore, HR-TEM, selected area electron diffraction (SAED), STEM, and color mapping based on EDX were employed to identify the nanocrystals as spinel cobalt oxide and to study their crystallinity in Co_3O_4 NC/N-CNT. XRD (Brunker AXS D8 Advance) was utilized to confirm the spinel crystal structure of cobalt oxide nanocrystals in Co_3O_4 NC/N-CNT, and XPS (Thermal Scientific K-Alpha XPS spectrometer) was implemented not only to verify the surface atomic composition of the developed material, but also to quantify the different configurations of nitrogen species. TGA was performed to elucidate the amount of Co_3O_4 NC in the hybrid.

Preparation of a glassy carbon electrode

A glassy carbon electrode (Diameter: 5 mm with surface area: 0.196 cm^2) was utilized as a working electrode. It was first polished by using alumina powder (size: 0.3 μm and 0.05 μm), and then the electrode was ultrasonicated directly in deionized water for a short time then dried in a nitrogen gas stream. To prepare the sample ink, the catalyst (4 mg) was put into ethanol (1 mL) pretreated by Nafion solution (0.05 wt%), and the mixture was ultrasonicated for 2 h to obtain a homogenously mixed ink. The as-prepared dispersion (20 μL) was dropped onto the circle-shaped glassy carbon and dried under ambient conditions (catalyst loading: 0.4 mg cm^{-2}).

Electrochemical measurements: Three-electrode half-cell testing

A RDE half-cell system was employed to investigate both the ORR and OER catalytic activity of the prepared materials. A conventional three-electrode system that consisted of a working electrode, counter electrode, and reference electrode was used. As described above, the catalyst-coated glassy carbon disk electrode and a Pt wire were used as the working and counter electrodes, respectively, and a SCE was employed as the reference electrode. KOH solution (0.1 M) was used as the aqueous electrolyte. To obtain an O_2- or N_2-saturated electrolyte, O_2 or N_2 was used to purge the KOH solution for 30 min before the evaluations, and bubbling was continued during the tests. The electrochemical activities of the materials were studied by CV for the OER and linear sweep voltammetry (LSV) for the ORR, which were performed by using a CHI Electrochemical Station (Model 760D) and a rotation speed controller (Pine Instrument Co., AFCBP-1). Catalytic activity towards the ORR was recorded from 0.1 to −1.0 V vs. SCE at a scan rate of 10 mV s^{-1} with O_2-saturated electrolyte under a series of rotating electrode speeds (400, 900, 1600, and 2500 rpm). The ORR polarization curves were corrected by subtracting background currents by the same test procedures obtained with a N_2-saturated electrolyte to remove capacitive contributions during the tests of ORR activities. The electrochemical performance of the OER was evaluated from 0–1 V vs. SCE at a scan rate of 10 mV s^{-1} (50 mV s^{-1} for the OER cycling as a durability test) with N_2-saturated electrolyte at 900 rpm to remove surface O_2 bubbles generated during the OER test. The precious-metal-based bifunctional active material that consisted of both Pt/C (28.8 wt% Pt), as one of the best ORR electrocatalysts, and Ir/C (20 wt% Ir), as one of the best OER catalysts, was employed as the reference material to demonstrate the superiority of the bifunctional Co_3O_4 NC/N-CNT hybrid material.

Fabrication of zinc–air battery single cell and performance evaluation

The practical use of the electrochemical catalyst was investigated by using a rechargeable zinc–air battery (ZAB) prototype, which consisted of an air electrode, zinc plate, electrolyte, and separator (Supporting Information, Figure S1). The air electrode was first prepared using a gas diffusion layer (GDL; Ion Power Inc., SGL Carbon 10 BB) upon which the catalyst was spray-coated by using an air brush with an air electrode active area of 0.785 cm^2.[18] The catalyst materials were dispersed in a Nafion-containing (5 wt%) isopropanol mixture with a catalyst concentration of 4 mg mL^{-1}. This mixture was then ultrasonicated for 1 h at RT to obtain a well-dispersed ink solution. Then, it was air-brush sprayed onto the GDL for subsequent testing (average catalyst/binder loading: 1 mg cm^{-2}). A polished zinc plate (OnlineMetals, Zinc Sheet EN 988), a microporous 25 μm polypropylene membrane (Celgard 5550), and 6.0 M KOH with 0.2 M zinc acetate solution were employed as the anode, separator, and electrolyte, respectively. Galvanodynamic discharge and charge experiments and EIS tests were performed by using a multichannel potentiostat (Princeton Applied Research, VersaSTAT MC). Discharge and charge profiles were obtained at a wide range of current change (current density: 0–60 mA cm^{-2}). The EIS was implemented with a fixed potential at 0.8 V and the frequency was changed from 100 000 to 0 Hz. All of the tests were conducted before and after cycles. Zinc–air battery single-cell cycling tests were performed by using a cycling tester (BTSDA). The cycling was performed with 10 min cycles (5 min discharge and 5 min charge) and a high current density of

© 2015 Wiley-VCH Verlag GmbH & Co. KGaA, Weinheim

20 mA cm^{-2}. For long cycle performance measurements in relatively harsh conditions, a long-term cycling test was conducted, in which one cycle was 4 h (2 h each for discharge and charge) at the same current density (20 mA cm^{-2}).

Acknowledgements

This research was supported by the Natural Sciences and Engineering Research Council of Canada (NSERC) through grants to Prof. Zhongwei Chen and the University of Waterloo.

Keywords: carbon · cobalt · electrochemistry · oxygen · supported catalysts

[1] Z.-L. Wang, D. Xu, J.-J. Xu, X.-B. Zhang, *Chem. Soc. Rev.* **2014**, *43*, 7746 – 7786.
[2] Y. Li, H. Dai, *Chem. Soc. Rev.* **2014**, *43*, 5257 – 5275.
[3] R. Cao, J.-S. Lee, M. Liu, J. Cho, *Adv. Energy Mater.* **2012**, *2*, 816 – 829.
[4] F. Cheng, J. Chen, *Chem. Soc. Rev.* **2012**, *41*, 2172 – 2192.
[5] C. Jin, F. Lu, X. Cao, Z. Yang, R. Yang, *J. Mater. Chem. A* **2013**, *1*, 12170 – 12177.
[6] Y. Liang, Y. Li, H. Wang, J. Zhou, J. Wang, T. Regier, H. Dai, *Nat. Mater.* **2011**, *10*, 780 – 786.
[7] H. W. Park, D. U. Lee, Y. Liu, J. Wu, L. F. Nazar, Z. Chen, *J. Electrochem. Soc.* **2013**, *160*, A2244 – A2250.
[8] J.-S. Lee, S. Tai Kim, R. Cao, N.-S. Choi, M. Liu, K. T. Lee, J. Cho, *Adv. Energy Mater.* **2011**, *1*, 34 – 50.
[9] F. Cheng, J. Liang, Z. Tao, J. Chen, *Adv. Mater.* **2011**, *23*, 1695 – 1715.
[10] D. Geng, Y. Chen, Y. Chen, Y. Li, R. Li, X. Sun, S. Ye, S. Knights, *Energy Environ. Sci.* **2011**, *4*, 760 – 764.
[11] L. Lai, J. R. Potts, D. Zhan, L. Wang, C. K. Poh, C. Tang, H. Gong, Z. Shen, J. Lin, R. S. Ruoff, *Energy Environ. Sci.* **2012**, *5*, 7936 – 7942.
[12] J.-S. Lee, T. Lee, H.-K. Song, J. Cho, B.-S. Kim, *Energy Environ. Sci.* **2011**, *4*, 4148 – 4154.
[13] Y. Li, M. Gong, Y. Liang, J. Feng, J. E. Kim, H. Wang, G. Hong, B. Zhang, H. Dai, *Nat. Commun.* **2013**, *4*, 1805.
[14] D. U. Lee, H. W. Park, M. G. Park, V. Ismayilov, Z. Chen, *ACS Appl. Mater. Interfaces* **2015**, *7*, 902 – 910.
[15] J. Masa, W. Xia, I. Sinev, A. Zhao, Z. Sun, S. Grutzke, P. Weide, M. Muhler, W. Schuhmann, *Angew. Chem. Int. Ed.* **2014**, *53*, 8508 – 8512; *Angew. Chem.* **2014**, *126*, 8648 – 8652.
[16] Y. Liang, H. Wang, P. Diao, W. Chang, G. Hong, Y. Li, M. Gong, L. Xie, J. Zhou, J. Wang, T. Z. Regier, F. Wei, H. Dai, *J. Am. Chem. Soc.* **2012**, *134*, 15849 – 15857.
[17] H. W. Park, D. U. Lee, P. Zamani, M. H. Seo, L. F. Nazar, Z. Chen, *Nano Energy* **2014**, *10*, 192 – 200.
[18] Z. Chen, A. Yu, D. Higgins, H. Li, H. Wang, Z. Chen, *Nano Lett.* **2012**, *12*, 1946 – 1952.
[19] M. Prabu, P. Ramakrishnan, S. Shanmugam, *Electrochem. Commun.* **2014**, *41*, 59 – 63.
[20] Z. Chen, A. Yu, R. Ahmed, H. Wang, H. Li, Z. Chen, *Electrochim. Acta* **2012**, *69*, 295 – 300.
[21] Y. Liang, Y. Li, H. Wang, H. Dai, *J. Am. Chem. Soc.* **2013**, *135*, 2013 – 2036.
[22] D. U. Lee, B. J. Kim, Z. Chen, *J. Mater. Chem. A* **2013**, *1*, 4754 – 4762.
[23] Y. Zhao, S. Chen, B. Sun, D. Su, X. Huang, H. Liu, Y. Yan, K. Sun, G. Wang, *Sci. Rep.* **2015**, *5*, 7629.
[24] C.-F. Chen, G. King, R. M. Dickerson, P. A. Papin, S. Gupta, W. R. Kellogg, G. Wu, *Nano Energy* **2015**, *13*, 423 – 432.
[25] M. Prabu, K. Ketpang, S. Shanmugam, *Nanoscale* **2014**, *6*, 3173 – 3181.
[26] G. S. Park, J.-S. Lee, S. T. Kim, S. Park, J. Cho, *J. Power Sources* **2013**, *243*, 267 – 273.
[27] D. Eder, *Chem. Rev.* **2010**, *110*, 1348 – 1385.
[28] N. Zhao, W. Nie, J. Mao, M. Yang, D. Wang, Y. Lin, Y. Fan, Z. Zhao, H. Wei, X. Ji, *Small* **2010**, *6*, 2558 – 2565.
[29] M. Glerup, M. Castignolles, M. Holzinger, G. Hug, A. Loiseau, P. Bernier, *Chem. Commun.* **2003**, 2542 – 2543.
[30] J. H. Lin, C. S. Chen, Z. Y. Zeng, C. W. Chang, H. W. Chen, *Nanoscale* **2012**, *4*, 4757 – 4764.
[31] C. Xiong, Z. Wei, B. Hu, S. Chen, L. Li, L. Guo, W. Ding, X. Liu, W. Ji, X. Wang, *J. Power Sources* **2012**, *215*, 216 – 220.
[32] P. Ayala, R. Arenal, M. Rümmeli, A. Rubio, T. Pichler, *Carbon* **2010**, *48*, 575 – 586.
[33] Y. Liu, D. C. Higgins, J. Wu, M. Fowler, Z. Chen, *Electrochem. Commun.* **2013**, *34*, 125 – 129.
[34] D. Higgins, Z. Chen, D. U. Lee, Z. Chen, *J. Mater. Chem. A* **2013**, *1*, 2639 – 2645.
[35] H. Kim, K. Lee, S. I. Woo, Y. Jung, *Phys. Chem. Chem. Phys.* **2011**, *13*, 17505 – 17510.
[36] T. Sharifi, G. Hu, X. Jia, T. Wagberg, *ACS Nano* **2012**, *6*, 8904 – 8912.
[37] D. U. Lee, J.-Y. Choi, K. Feng, H. W. Park, Z. Chen, *Adv. Energy Mater.* **2014**, *4*, 1301389.
[38] D. R. Lawson, L. D. Whiteley, C. R. Martin, M. N. Szentirmay, J. I. Song, *J. Electrochem. Soc.* **1988**, *135*, 2247 – 2253.
[39] S. K. Zecevic, J. S. Wainright, M. H. Litt, S. L. Gojkovic, R. F. Savinell, *J. Electrochem. Soc.* **1997**, *144*, 2973 – 2982.
[40] W. Yuan, Y. Zhou, Y. Li, C. Li, H. Peng, J. Zhang, Z. Liu, L. Dai, G. Shi, *Sci. Rep.* **2013**, *3*, 2248.
[41] A. K. Geim, *Science* **2009**, *324*, 1530 – 1534.
[42] H. Dai, *Acc. Chem. Res.* **2002**, *35*, 1035 – 1044.
[43] X. Wang, J. Zhuang, Q. Peng, Y. Li, *Nature* **2005**, *437*, 121 – 124.
[44] Z. Chen, Y. Yuan, H. Zhou, X. Wang, Z. Gan, F. Wang, Y. Lu, *Adv. Mater.* **2014**, *26*, 339 – 345.

Received: May 6, 2015
Revised: June 18, 2015
Published online on August 13, 2015

© 2015 Wiley-VCH Verlag GmbH & Co. KGaA, Weinheim